

A BUBBLE-POWERED MICRO-ROTOR: MANUFACTURING, ASSEMBLY AND CHARACTERIZATION

Jonathan Kao*, John Warren**, Jie Xu*** and Daniel Attinger***

*State University of New York, Stony Brook NY 11794-2300

** Brookhaven National Laboratory, Upton NY 11973

***Columbia University, New York NY 10027, da2203@columbia.edu

ABSTRACT

This paper demonstrates experimentally the feasibility of a novel micro-rotor actuation concept. We demonstrate how a fluid flow, created by the interactions between a bubble and acoustic waves, can be exploited to assemble and power a micro-rotor at a speed as high as 625 rpm. The 65 μm micro-rotor is manufactured in SU-8 using photolithography, all inspired by a biological structure: the winged seed of the maple tree. Variables controlling the rotation speed are investigated, such as the bubble diameter, the acoustic excitation amplitude and frequency, as well as the rotor geometry. The extractible power is estimated to be in the femtowatt range. Finally, steps are outlined to develop this micro-rotor into a MEMS-based motor delivering tunable, rotary power at the microscale.

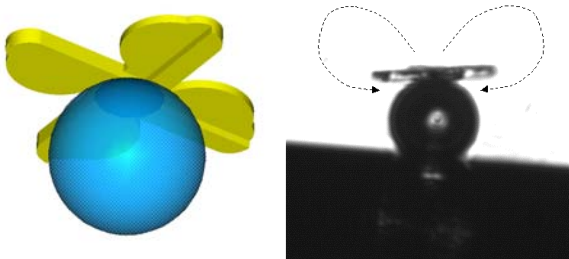


Figure 1: 3D Model of the rotor actuation system (left), and frame extracted from a high-speed visualization (right). Superimposed dashed lines have the approximate shape of the streamlines. Rotor diameter is 65 μm .

1. INTRODUCTION

Development of MEMS-based micro-motors is needed for biomedical applications such as drug delivery systems, surgical tools, probes [1] and bio-mechanical actuators for biological

cells [2]. Challenges towards the development of such applications include the improvement of efficiency, as well as the precise control of the power curve through tunable torque and rotation speed. Since the 1990s, significant efforts have been produced on developing MEMS-based micro-motors. A first approach is to miniaturize an existing macroscopic concept. For instance, micro gas turbines [3-5], a miniature Wankel engine [6], as well as electrostatic micro-motors [1] have been built with photolithographic processes. These prototypes are yet outstanding because of their complexity and high power density, on the order of $100\text{MW}/\text{m}^3$. However, this miniaturization approach involves inherent difficulties, because the ratio of surface forces to volume forces is proportional to the inverse of the device size. As a result, friction, wear and geometric tolerance issues that are manageable at large scales become annoying at the microscale. A second approach is to take advantage of this different ratio of forces in the microscale world. Designs of great simplicity can be produced this way, as exemplified by the bubble-jet printing technology, where an explosive bubble acts as a piston [7]. It must be stated that design simplicity sometimes goes along with complex thermo-fluid phenomena [8], because of the strong coupling of transport phenomena, and the very small time and space scales involved. Recently, our group presented preliminary experiments showing that an acoustic bubble can induce a steady rotation to an object in contact with the bubble [9]. This novel rotor actuation concept will allow the realization of a micro-motor using acoustic waves to produce rotary power. The contribution of the present study is to use rotors with controlled, engineered shapes, to prove that they can also rotate on top of the bubble, and to characterize several parameters controlling the rotation stability and speed.

The rotor activation concept presented here uses the small, linear oscillations of a bubble in a standing ultrasonic wave, as follows. When a free-floating bubble is excited by ultrasound, its volume oscillates according to the Rayleigh-Plesset equation [10], and the surrounding liquid participates to these oscillations with a symmetrical, radial motion. In the case where the oscillating bubble is attached to a solid wall, as in the proposed concept, the motion of the surrounding liquid is not radially-symmetrical anymore: the bubble-liquid interface exhibits a coupling of radial and translational motion, through respective expansion (or contraction) and translation perpendicular to the wall. As a consequence, a second order, steady vortical fluid flow appears in the immediate vicinity of the bubble - a phenomenon called microstreaming, recently investigated theoretically [11] and exploited in biological applications to manipulate biological cells [12]. In [9], the low-Reynolds number fluid flow is simulated by superposing potential solutions for Stokes flow, and provides a valid stream function for the problem of the acoustic streaming of a bubble close to a stationary wall. The general shape of the streamlines around a bubble are superposed to the photograph in Figure 1, as a donut-shaped, vortical flow structure with main symmetry axis perpendicular to the surface where the bubble sits. The analytical solution agrees well with flow visualization utilizing particles as tracers [9], and the maximum velocity magnitude is on the order of 1 mm/s. In this article, we describe the manufacturing and actuation of the micro-rotors, as well as how a microstreaming flow is used to position the MEMS-based micro-rotor on top of the bubble and induce its rotation.

2. MICRO-ROTORS DESIGN AND MANUFACTURING

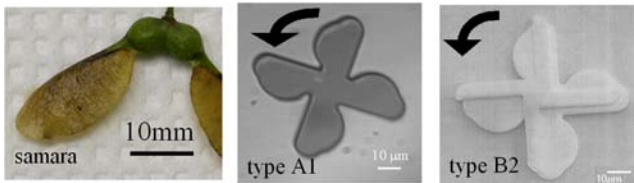


Figure 2: Geometry of the maple tree fruit or samara (left), which inspired the micro-rotors used in this study. Type A1 is a monolayer rotor, while type B2 rotors feature two layers to mimic the samara vein.

We micro-manufactured three types of micro-rotors, shown in Figure 2, each with a diameter of 65 µm. The rotors mimic the general shape of the maple tree fruit. They have either a single layer (A1 batch), or two layers (A2, B2) to better reproduce the non-planar structure of the winged seed. The micro-rotors were fabricated using optical lithography to pattern SU-8, an epoxy-based photoresist used to fabricate high aspect ratio microstructures for MEMS applications. The slight misalignment between the two layers seen in rotors of batch B2 comes from the delicate optical alignment of the second mask with respect to the first. The other 2-layer batch, A2, had a significantly larger misalignment. The thickness of the rotors was measured with a Dektak profilometer to be 1.87

µm for the A1 type. The B2-type micro-rotors had a thickness of 1.98 µm for the layer in contact with the bubble (see Figure 1), and for the second layer a thickness of 2.20 µm.

3. EXPERIMENTAL SETUP

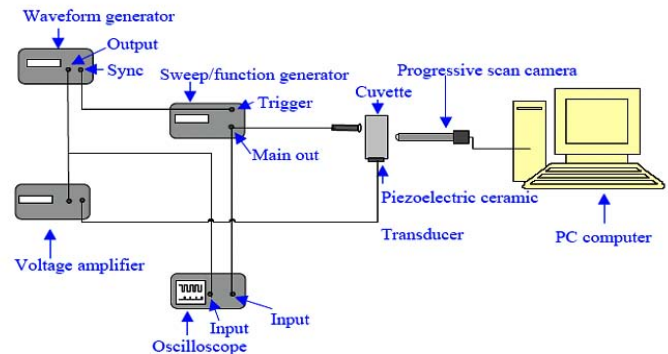


Figure 3: Experimental setup. The function and waveform generator are used to drive the illumination and piezoelectric excitation. The cuvette contains the micro-heater (not pictured) where the bubble is formed.

The experimental setup is pictured in Figure 3. The heart of the experimental setup consists of a 10 mL glass cuvette, with a piezoelectric ceramic transducer glued at its bottom. The transducer allows controlling a standing pressure wave in the fluid contained in the cuvette. A resistance microheater is placed in the cuvette to generate on its surface isolated micro-bubbles, by gas desorption from the gently heated liquid. When the cuvette is filled with water, the temperature increase in the fluid can be estimated using the first law of thermodynamics:

$$\rho V c_p \Delta T = U I t \quad (2)$$

In our setup, $V = 10$ mL, $U = 5$ V and $I = 0.5$ A. Using the physical properties of water and a heating time of 5 s, we calculated an average temperature rise in the fluid of $\Delta T = 0.3$ K, which is negligible. A 15 MHz waveform generator connected to a voltage amplifier (Krohn-Hite 7600 M, 200 V) drives the oscillations of the piezoelectric transducer (the voltage applied to the piezoelectric transducer will be referred to as V_{trans} throughout the rest of this paper). The largest bubble oscillations appear when the excitation frequency matches both the natural frequency of the cuvette [13] and the natural bubble frequency [10]. The dynamics of the bubble is observed with a high-speed camera, a microscope and a photodiode, at a spatial resolution of 1 µm and frame rates from 20 to 330 fps.

4. ASSEMBLY OF THE MICRO-ROTOR ON TOP OF THE BUBBLE

Positioning a micro-rotor on top of a micro-bubble is not a trivial task when both objects have sizes below 100 μm . Fortunately, the microstreaming flow field could be used to self-assemble a rotor on top of the bubble, according to the following procedure. The cuvette was filled with a solution containing hundreds of micro-rotors. The viscosity of the solution, measured with a Brookfield viscometer, was 1.1 ± 0.1 cP, close to the viscosity of water. The rotors were efficiently mixed through the generation of acoustic waves in the cuvette. When micro-rotors came in the vicinity of a micro-bubble, a micro-rotor would be attracted by the vortical flow shown in Figure 1, and would position itself on top of the micro-bubble, where it would then self-center, probably because of the symmetrical flow structure. The micro-rotor would then rotate on top of the micro-bubble, with the axis of rotation perpendicular to the solid surface where the bubble sits. The typical time frame from the appearance of a micro-rotor in the vicinity of the bubble to its actuation on the micro-bubble is 2 seconds. Probably, the interaction between the symmetrical flow pattern and the asymmetrical rotor is responsible for the rotation of the rotor. Also, the observed rotation was consistently in the direction indicated by an arrow in Figure 2.

5. CHARACTERIZATION OF THE BUBBLE-BASED ROTOR EXCITATION CONCEPT

The best way to fully understand the complex interaction between the fluid flow and the rotor-bubble system is to compare numerical simulations with different experimental conditions. To this end, our study has identified the following parameters that influence the rotation speed n and the angle α between the rotor plane and the solid surface plane: the micro-bubble radius a , the driving ultrasonic frequency f , the voltage applied to the piezoelectric transducer V_{trans} and the micro-rotor geometry (type A1, A2 or B2, see Figure 2). In our study, the rotation speed and angle were obtained by optical examination of frames extracted from the high-speed visualization. The effect of the *bubble radius* on the rotation speed was tested at a constant ultrasonic frequency (161.4 kHz, the natural frequency of the cuvette) and voltage (70 V), with B2-type rotors, for radiuses between 21 and 24 μm . It appears that the rotation frequency decreases as the bubble size increases. Very likely, this phenomenon can be explained by considering the relation [10] between the bubble radius a and oscillation frequency f_b :

$$a \cdot f_b = 3m/s \quad (3)$$

This equation predicts that the radius of a bubble maximizing the micro-streaming energy for an excitation frequency at 161.4 kHz is 19 μm . The observed relation between the bubble radius and the rotor rotation frequencies has very likely been obtained with bubbles larger than their optimum size, i.e. with bubbles having a natural frequency lower than the excitation frequency. We were not able to obtain

data for the other part of the resonant curve, because interfacial diffusion through the membrane increases for smaller bubbles [10] and caused the bubbles to shrink and disappear within minutes. It appears therefore that the optimum bubble size depends on the need to match the bubble natural frequency to the cuvette frequency, as well as the need to minimize interfacial diffusion. As a consequence, we found that the optimum bubble size to be about 20 μm .

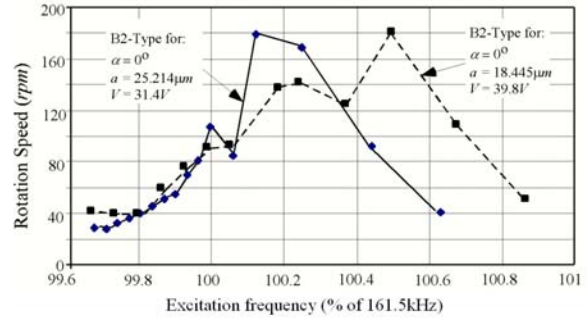


Figure 4: Influence of the excitation frequency on the rotational speed using B2-type rotors. The speed is measured from high-speed visualizations.

The *frequency* response of several micro-rotors was assessed by varying the frequency of the acoustic excitation in the vicinity of the frequency maximizing the rotation speed. Figure 4 depicts the respective frequency response of micro-rotors of type A1, A2 and B2. Clearly, the frequency increases drastically when it matches the resonant frequency of the system, which is the natural frequency the cuvette (which depends on the cuvette shape and fluid properties [13]). The sensitivity to the excitation frequency is high, which is interesting since excitation frequency is a parameter easy to control. The frequency response curve is analogous to the frequency response of linear spring-inertia-dashpot system [14], where the response is relatively constant for under-critical excitation frequencies, peaks at the natural frequency, and vanishes for over-critical excitation frequencies. In the system described here, the surface tension is the spring, and the inertia and dashpot correspond to the complex fluid motion and interaction with the propeller. In the case of the micro-rotor, over-critical excitation frequencies would correspond to cases where the rotor stops turning. The rotation speed increases monotonically with the transducer *voltage* V_{trans} , which can be explained by the fact that the energy delivered to the system increases. A linear regression best fit of the experimental data for A2-geometry gives the following best-fit equation

$$n = 6.18V_{trans} - 311 \quad (4)$$

where n is the rotation speed in revolutions per minute and V is the amplifying voltage in volts. It must be noted that more direct ways exist to measure the energy delivered to the system,

such as a needle hydrophone, but this device was not available for our measurements.

The rotor geometry (see Figure 2) influences its rotation in three ways: the regularity of the rotation, the rotation angle α between the rotor plane and the solid surface plane, and the rotation speed. Measurements evaluated α and the spin regularity for three types of micro-rotors. Generally a large value of alpha would correspond to unstable rotation and early detachment of the rotor from the micro-bubble. B2-type micro-rotors always spin with $\alpha = 0$ and with a high regularity. A2-type rotors typically rotate with an angle of 15 to 30 degree, probably due to their larger misalignment, but never span erratically. Rotor of type A1 were also observed behaving erratically, e.g. making a revolution one direction, and then a revolution in the reverse direction, “rocking” all over the surface of the bubble. The maximum rotation speeds reached during our measurement campaign were 33rpm, 300rpm and 625 rpm for the A1, B2 and B2 rotors, respectively. It appears therefore that the geometry is a critical parameter for rotor stability and rotation speed. Also, the two-layer design (more accurately resembling the winged seed in Figure 2, and exhibiting a more asymmetric shape) is more stable and turns 10 to 20 times faster than a monolayer design. Another important result is that misalignment should be minimized for stability and efficiency purposes, as exemplified by the faster rotation speed of rotor B2 versus A2. Optimizing the rotor geometry and manufacturing is therefore critical to maximize rotation speed and extractable power, and the measurements describe in this article can serve as a basis for numerical simulations to develop a next generation of optimized micro-rotors.

6. FROM A MICRO-ROTOR TO A MICRO-MOTOR

At such low Reynolds number, the power given by the fluid to the rotor is approximately equal to the viscous dissipation that would be produced by the rotation of a similar rotor, at a similar speed, in a quiescent fluid. Von Karman obtained the exact solution of the laminar flow created by a rotating disk, and the torque M on one side of the disk is [15]

$$M = 0.62 \frac{\pi}{2} \rho a^4 \sqrt{\nu \omega^3} \quad (5)$$

where ρ and ν are the respective density and kinematic viscosity of the surrounding fluid. The rotary power P can therefore be estimated as

$$P = 2M\omega \quad (6)$$

Using the physical properties of water, the radius of the manufactured rotor and a rotation speed of $\omega=65/s$, corresponding to a rotation at 625 rpm, we obtain from the two above equations that the power $P=74$ femtowatt. The question of how to extract this rotary power from the micro-rotor can be addressed as follows. A sub-micrometer diameter shaft could be attached perpendicularly to the rotor to transmit the mechanical power through the bubble and the solid wall. Multi-wall carbon nanotubes can be used to build the shaft, since

these tubes have sub-micrometer diameter, and very low relative friction. The outer tube will then be glued to the wall where the bubble sits, while the inner tube will be attached to the rotor. Alternatively, biofibers can be used. It must be stressed that the proposed motor is simple enough to be scaled further down, provided the bubble is sufficiently stable to degassing [10], an issue that can be addressed with surfactants and use of different gases and liquids. Two packaging solutions for the motor are presented in Figure 5: since only one dimension needs to be conserved to induce the acoustic wave with a desired frequency, concentric geometries can be investigated to minimize the total volume. Also, Figure 5b shows that several motors can be fitted in series in a space as thin as a human hair. Finally, the remote activation (through acoustic wave) allows the design and activation of several micro-motors in parallel.

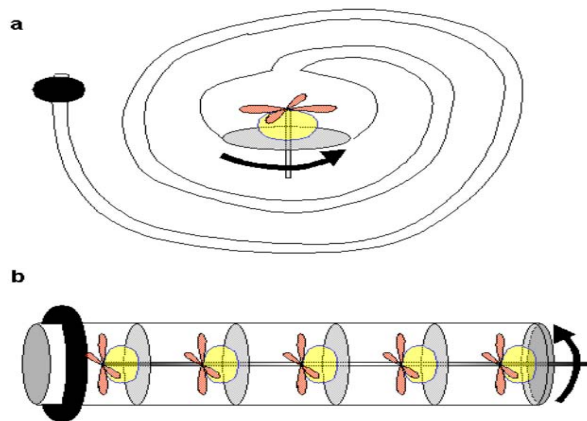


Figure 5: Tentative packaging of the micro-motor. The thick ring at the top is a piezoelectric transducer. In (a), a concentric geometry reduces the volume. In (b), five motors in series drive a unique shaft.

7. CONCLUSIONS

The feasibility of an acoustic, bubble-based excitation concept for a micro-rotor has been demonstrated. The steady, vortical flow field created by the oscillations of the micro-bubble is used to position the rotor on top of the micro-bubble, and induce its steady rotation. The main variables controlling the rotation speed are: the bubble radius, the excitation frequency and voltage, and the rotor geometry. The very high sensitivity to the excitation frequency provides an easy way to control the rotation speed. Measurements show that the response of the rotor to the excitation is analogous to the frequency response of a linear spring-inertia-dashpot system. Finally, experiments with three well-defined rotor shapes open the way to numerical simulations that will allow (1) a better understanding of the transformation of the microstreaming flow field into rotary energy, and (2) a further optimization of the rotor shape. These necessary steps will allow the manufacturing of a micro-motor that is able to apply a controllable, infinitesimal torque at the microscale.

ACKNOWLEDGMENTS

This research was carried out in part at the Center for Functional Nanomaterials, Brookhaven National Laboratory, which is supported by the U.S. Department of Energy, Division of Materials Sciences and Division of Chemical Sciences, under Contract No. DE-AC02-98CH10886. Jonathan Kao was supported by the Simon's fellowship program at Stony Brook University. The authors thank Howard Stone, from Harvard University, for useful discussions.

REFERENCES

1. Chapman, P.L. and P.T. Krein, *Smaller is Better? Perspective on Micro-motors and Electric Drives*. IEEE Industry Applications Magazine, 2003: p. 62-67.
2. Marmottant, P. and S. Hilgenfeldt, *A bubble-driven microfluidic transport element for bioengineering*. Proceedings National Academy of Sciences, 2004. 101(26): p. 9523-9527.
3. Peirs, J., D. Reynaerts, F. Verplaetsen, F. Norman, and S. Lefever. *Development of a micro gas turbine for electric power generation*. in *MME 2003, The 14th MicroMechanics Europe Workshop*. 2003.
4. Epstein, A.H. *Millimeter-scale, MEMS gas turbine engines*. in *Proceedings of ASME Turbo Expo 2003, Power for Land, Sea, and Air*. 2003.
5. Fréchette, L.G., S.A. Jacobson, K.S. Breuer, F.F. Ehrich, R. Ghodssi, R. Khanna, C.W. Wong, X. Zhang, M.A. Schmidt, and A.H. Epstein, *High-Speed Microfabricated Silicon Turbomachinery and Fluid Film Bearings*. J. Microelectromechanical Systems, 2005. 14(1): p. 141-152.
6. Fu, K., A. Knobloch, F. Martinez, D.C. Walther, A.C. Fernandez-Pello, A.P. Pisano, and D. Liepmann, *Design and Fabrication of a Silicon-Based MEMS Rotary Engine*, in *Proc. ASME 2001 International Mechanical Engineering Congress and Exposition (IMECE), MEMS division*. 2001, ASME, New York: New York, NY.
7. Chen, P., W. Chen, P. Ding, and S. Chang, *Droplet formation of a thermal sideshooter inkjet printhead*. International Journal of heat and fluid flow, 1998. 19(4): p. 382-390.
8. Glod, S., D. Poulidakos, Z. Zhao, and G. Yadigaroglu, *An Investigation of Microscale Explosive Vaporization of Water on an Ultrathin Pt Wire*. Int. J. Heat and Mass Transfer, 2002. 45: p. 367-379.
9. Wang, X., F. Moraga, and D. Attinger, *A micro-rotor driven by an acoustic bubble*. Microscale Thermophysical Engineering. accepted for publication, July 2005.
10. Leighton, T.G., *The acoustic bubble*. 1994: Academic Press, London.
11. Longuet-Higgins, M.S., *Viscous streaming from an oscillating spherical bubble*. Proc. R. Soc. Lond. A, 1998. 454: p. 725-742.
12. Marmottant, P. and S. Hilgenfeldt, *Controlled vesicle deformation and lysis by single oscillating bubbles*. Nature, 2003. 423: p. 153-156.
13. Blackstock, D.T., *Fundamentals of Physical Acoustics*. 2000: Wiley, New York.
14. Meirovitch, L., *Fundamentals of Vibrations*. 2001: McGraw-Hill: New York, NY.
15. White, F., *Viscous Fluid Flow*. 3rd ed. 2006: McGraw Hill.